Ca2MnO3X (X = Cl, Br) Oxyhalides with 1-Dimensional Ferromagnetic Chains of Square-Planar S = 2 Mn3+

Fabio Denis Romero, Christophe Lepoittevin, Stéphanie Kodjikian, Claire Colin, Michael Hayward

Ca_2MnO_3X (X = Cl, Br) – Oxyhalides with 1-dimensional ferromagnetic chains of square planar S = 2 Mn^{3+}

Fabio Denis Romero,*[1] Christophe Lepoittevin,[1] Stéphanie Kodjikian,[1] Claire V. Colin,[1] Michael A. Hayward[2]

1. Univ. Grenoble Alpes, CNRS, Grenoble INP, Institut Néel, 38000 Grenoble, France
2. Inorganic Chemistry Laboratory, Department of Chemistry, University of Oxford, South Parks Road, Oxford OX1 3QR, United Kingdom

ABSTRACT: Mixed anion oxyhalides with formula Ca_2MnO_3X (X = Cl, Br) are synthesized using solid state reaction methods. These two materials crystallize in a novel structure type due to the small ionic radius of Ca and the strong Jahn-Teller effect of Mn^{3+}. The resulting structure (space group *Cmcm*) contains 1-dimensional chains of MnO_4 square planes, with an angle ~120 ° between neighboring planes. At low temperatures, the two materials adopt magnetic arrangements with ferromagnetic chains coupled antiferromagnetically. On applying a magnetic field, both materials experience spin flop transitions.

Introduction

Mixed anion compounds are solid state materials containing more than one anionic species. These compounds are much less explored than the families of monoanionic materials such as oxides. However, mixed anion materials offer the possibility of forming heteroleptic coordination polyhedra which can result in significantly different emergent properties. Furthermore, the differences in charge, ionic radius, electronegativity, and polarizability add new degrees of freedom with which to control and tune the electronic and atomic structure of these materials.[1]

Mixed systems containing oxide and heavy anions such as S, Se, Cl, Br, etc… tend to adopt layered structures. There are a large number of known oxyhalide materials with general formula $Sr_2M^{3+}O_3X$ (M = V, Mn, Fe, Co, Ni) with structures based on the n = 1 Ruddlesden-Popper (RP) structure type. In these materials, the chloride or bromide anions preferentially occupy the apical sites in an ordered fashion, and they are typically antiferromagnetic insulators due to the 180 ° M-O-M superexchange interaction within each layer.[2–9]

This tendency can be overcome by using ions with particular radius or coordination constraints. For example, the $A_3Fe_2O_5Cl_2$ series of phases adopt structures analogous to the n = 2 RP phases with apical chlorides for A = Ca and Sr, while for A = Ba, the structure contains a complex network of corner-sharing FeO_4 tetrahedra.[10,11] This is due to the much larger ionic radius of Ba, which cannot be easily accommodated in the n = 2 RP structure.

Particular coordination requirements can also overcome the tendency to form layered structures. For example, $M^{3+}OCl$ phases form for M = V, Ti, Cr, and Fe and adopt layered structures where the M cations are octahedrally coordinated by four oxides and two chlorides, the latter of which are cis arranged.[12–15] In contrast, attempting to prepare an analogous material with Jahn-Teller active d^4 Mn^{3+} results in a material with formula $Mn_8O_{10}Cl_3$ which adopts a complex 3-dimensional structure with Mn^3 cations in axially elongated octahedral environments with trans halide anions.[16]

These two effects can be exploited to prepare novel materials adopting unconventional crystal structures. Here, we report the synthesis, structure, and magnetic properties of $Ca_2Mn^{3+}O_3X$ (X = Cl, Br). The Jahn-Teller effect of the Mn^{3+} cations and the structural distortion necessary to accommodate the small Ca^{2+} leads these materials to crystallize in a novel structure type containing 1-dimensional chains of corner-sharing MnO_4 square planes. At low temperatures, both materials adopt long range antiferromagnetic order with antiparallel arrangement of ferromagnetic chains.

Experimental

Samples of Ca_2MnO_3X (X = Cl, Br) were prepared from suitable stoichiometric mixtures of CaO (99.95%), MnO_2 (99.99%) and MnX_2 (prepared from 99.9% $MnX_2{\cdot}4H_2O$ dried at 220 °C under dynamic vacuum over P_2O_5). The reagents were stored and handled in an argon-filled glove box and ground together using an agate mortar and pestle.

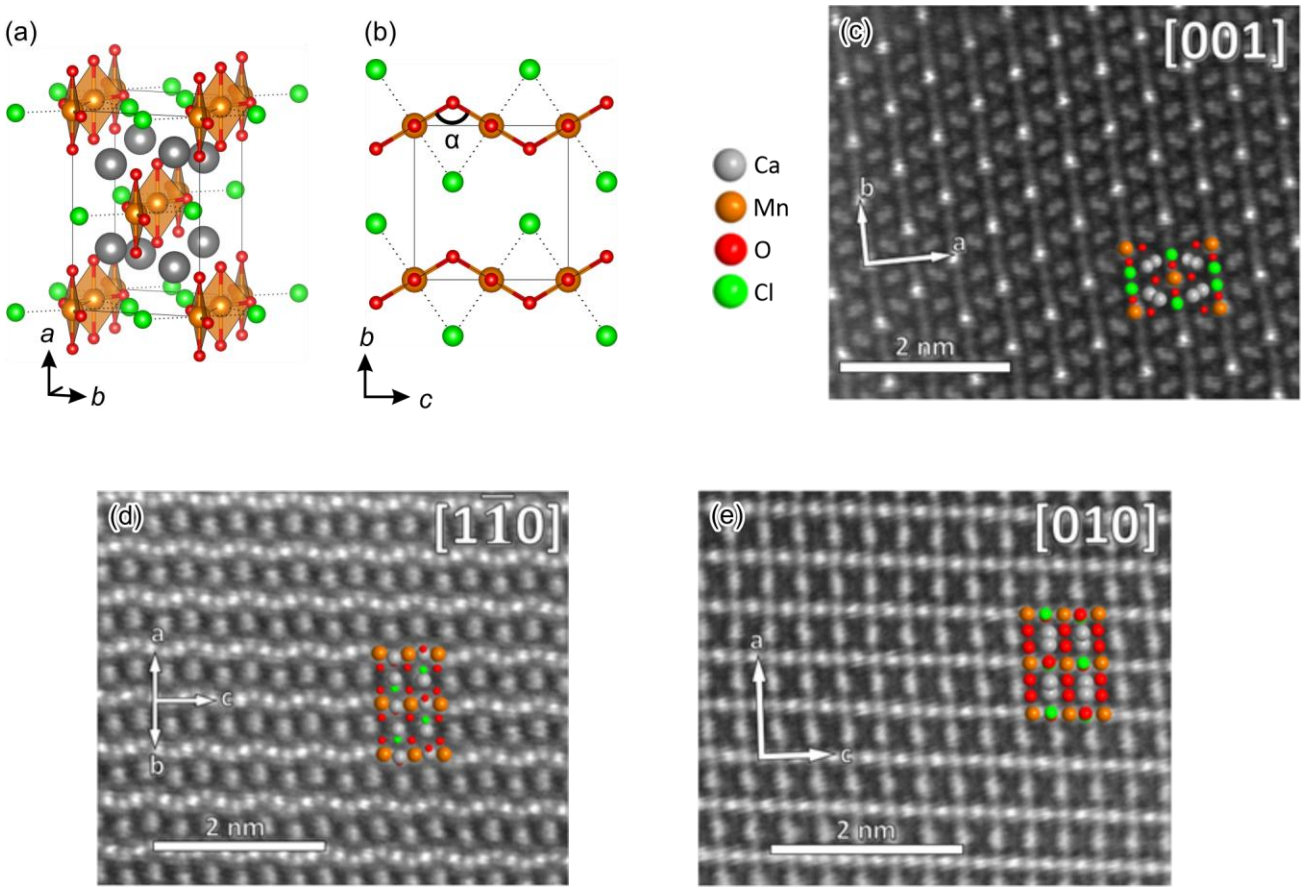

Figure 1. (a) and (b) Crystal structure of Ca_2MnO_3Cl. (c-e) [001], [1$\bar{1}$0] and [010] HAADF-STEM images recorded on Ca_2MnO_3Cl. The corresponding orientation of the refined structure is superimposed on it.

The resulting precursor powders were placed in quartz ampules and sealed under vacuum. These were then heated at 800 °C for two periods of 12 hours with an intermediate grinding. The resulting orange powders were found to be moisture sensitive and were therefore handled and stored in a glove box under an argon atmosphere (O_2 and H_2O < 0.5 ppm). Laboratory X-ray powder diffraction data were collected using a Bruker D8 Endeavor diffractometer with Cu Kα radiation.

Structure solution was carried out by transmission electron microscopy (TEM). A small amount of finely ground Ca_2MnO_3Cl was suspended in ethanol and a drop was deposited on a holey carbon membrane supported by a copper grid. 3D electron diffraction (3D-ED), high angle annular dark field scanning electron microscopy (HAADF-STEM), and energy dispersive X-ray (EDX) spectroscopy were performed using a JEOL NEOARM 200F operating at 200 kV. This microscope is equipped with a Nanomegas Digistar precession device and a 4K Gatan One View CMOS camera. The 3D-ED data were collected by recording non-oriented diffraction patterns during a step-by-step rotation of the sample holder (1° steps). A precession of 1.15° was applied in order to integrate the whole intensity of the diffracted reflections. The PETS2.0 software package was used to analyze the data and reconstruct the 3-dimensional reciprocal space.[17] The structural model of Ca_2MnO_3Cl was calculated using the charge flipping algorithm with the Superflip program as implemented in JANA2020.[18–20]

Magnetization measurements were performed using a Quantum Design MPMS XL SQUID magnetometer. Neutron powder diffraction data were collected using the D1b diffractometer at the Insitut Laue Langevin neutron source (Grenoble, France) from samples contained in vanadium cans sealed with indium washers. Refinements of the nuclear and magnetic structures of both compounds were carried out against combined data collected using neutron wavelengths of 2.53 and 1.29 Å.

Results

Structure Determination

EDX analysis carried out on 10 separate crystallites yielded the ionic ratio $Ca_{2.0(1)}Mn_{1.3(1)}Cl_{0.7(1)}O_x$. The unit cell identified from 3-dimensional reciprocal space reconstruction from 3D-ED data was orthorhombic with lattice parameters a = 10.4 Å, b = 6.8 Å, and c = 6.9 Å. Extinction conditions were determined from selected sections of the reciprocal space. Indexation of these sections yielded the systematic extinction conditions hkl: $h+k = 2n$ and $h0l$: $l = 2n$, consistent with orthorhombic space group *Cmcm* (Figure S 1).

Charge flipping was carried out using 406 independent reflections, yielding a completeness of 99.9% at a resolution of d = 0.75 Å. The 3-dimensional electrostatic potential map was interpreted by JANA2020 on the basis of the composition Ca_2MnO_3Cl (Figure S 2) to yield the structural model shown in Figure 1 (a) and (b). The model was confirmed and validated by Rietveld refinement against laboratory X-ray powder diffraction data (Figure S 3 (a)). An analogous model replacing Cl by Br could also be refined against laboratory X-ray powder diffraction data collected from Ca_2MnO_3Br (Figure S 3 (b)). In both cases, laboratory X-ray powder diffraction data showed additional reflections consistent with small (<2% by mass total) amounts of impurity phases (primarily Ca_2MnO_4).

The structural model was also confirmed by HAADF-STEM images. In these, the intensity of a projected column of ions is proportional to Z^n ($1 < n < 2$) where Z is the average atomic number (i.e. the brightest spots will correspond to the heaviest species: $Z_{Mn} = 25 > Z_{Ca} = 20 > Z_{Cl} = 17 > Z_O = 8$). Figure 1 (c-e) shows HAADF-STEM images along [001], [1$\bar{1}$0] and [010], along with the projections of the structural model refined against laboratory X-ray powder diffraction data. The good match between the refined model and HAADF-STEM images clearly indicate the accuracy of the structural model.

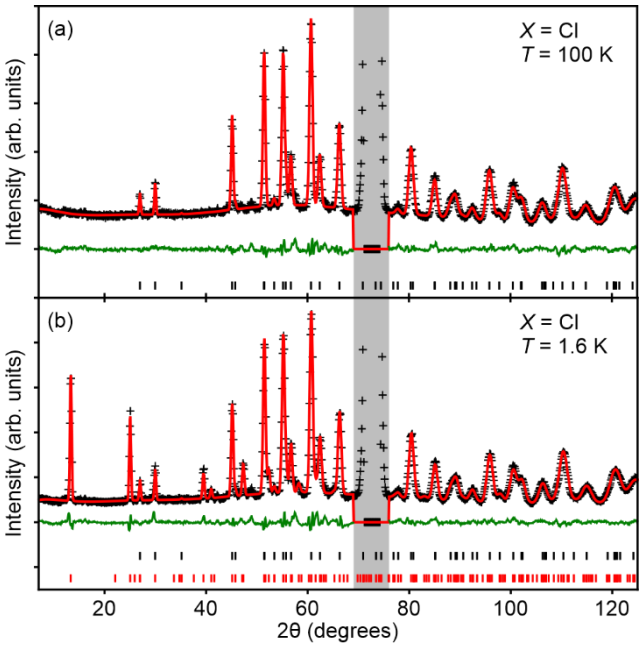

Figure 2. Observed, calculated and difference plots for the refinements of Ca_2MnO_3Cl against neutron powder diffraction data (λ ~ 2.53 Å). The black tick marks correspond to contributions from the nuclear structure and red to magnetic reflections. The shaded area corresponds to a portion of the data with a malfunctioning detector which was excluded from the refinement.

The refined structure contains chains of square planar coordinate Mn^{3+} cations along the [001] direction. These planes share corners, and are arranged such that the angle α between neighboring planes is ~ 120 °. Each chain has six nearest neighbor other chains, two of which are separated by halide ions along [010] and the other four by Ca cations.

Neutron powder diffraction collected from both materials at 100 K could be well accounted-for using the nuclear structure determined from TEM. Observed, calculated, and difference plots for the refinements against data with λ = 2.53 Å are shown in Figure 2 (a) and S 6. Observed, calculated, and difference plots for the refinements against data with λ = 1.29 Å are given in the Supporting Information. The refined parameters are given in Table 1 and in the Supporting Information.

Table 1. Structural parameters of Ca_2MnO_3Cl refined against neutron powder diffraction data collected at 100 K.

Atom	*x*	*y*	*z*	frac	U_{iso} / Å^2
Ca1	0.2870(3)	0.2176(5)	0.25	1	0.021(2)
Mn1	0	0	0	1	0.013(6)
O1	0	0.8507(8)	0.25	1	0.008(2)
O2	0.8026(3)	0	0	1	0.018(1)
Cl1	0	0.3587(5)	0.25	1	0.013(1)
Space group: *Cmcm* *a* = 9.7520(7) Å, *b* = 6.4946(4) Å, *c* = 6.5763(4) Å vol. = 416.51(7) Å^3					
χ^2 = 14.1, wRp = 4.30 %					

Magnetic Properties

Zero-field (ZFC) and field cooled (FC) magnetization data collected from both Ca_2MnO_3X materials as a function of temperature under an applied field of 100 Oe are shown in Figure 3 (a) and (b). Fits of the ZFC data to the Curie-Weiss law in the range 65-300 K yielded values of values of C = 3.23 emu K / mol and 3.04 emu K / mol (corresponding to μ_{eff} = 5.09 μ_B and 4.93 μ_B vs. an expected spin only μ_{exp} = 4.90 μ_B for S = 2 Mn^{3+}) and θ = 22 K and 19 K for X = Cl and Br respectively. The positive Weiss temperature in both compounds indicate that ferromagnetic interactions dominate.

Data collected from both materials contain a local maximum at T ~ 45 K. This feature is a consistent with the presence of a small amount of ferrimagnetic γ-Mn_2O_3. Below this temperature, both materials show features which are consistent with long range antiferromagnetic (AFM) ordering (T_N ~ 20 and 28 K for X = Cl and Br respectively).

Isothermal magnetization data collected from both materials at 300 and 5 K are shown in Figure 3 (c). In both cases, data are linear through the origin at 300 K. At 5 K, both materials show metamagnetic behavior with shapes characteristic of a spin flop transition. The critical fields for the two compounds are significantly different: H_C ~ 2.0 and 4.8 T for X = Cl and Br. In both cases, saturation is not reached at 5 T.

.

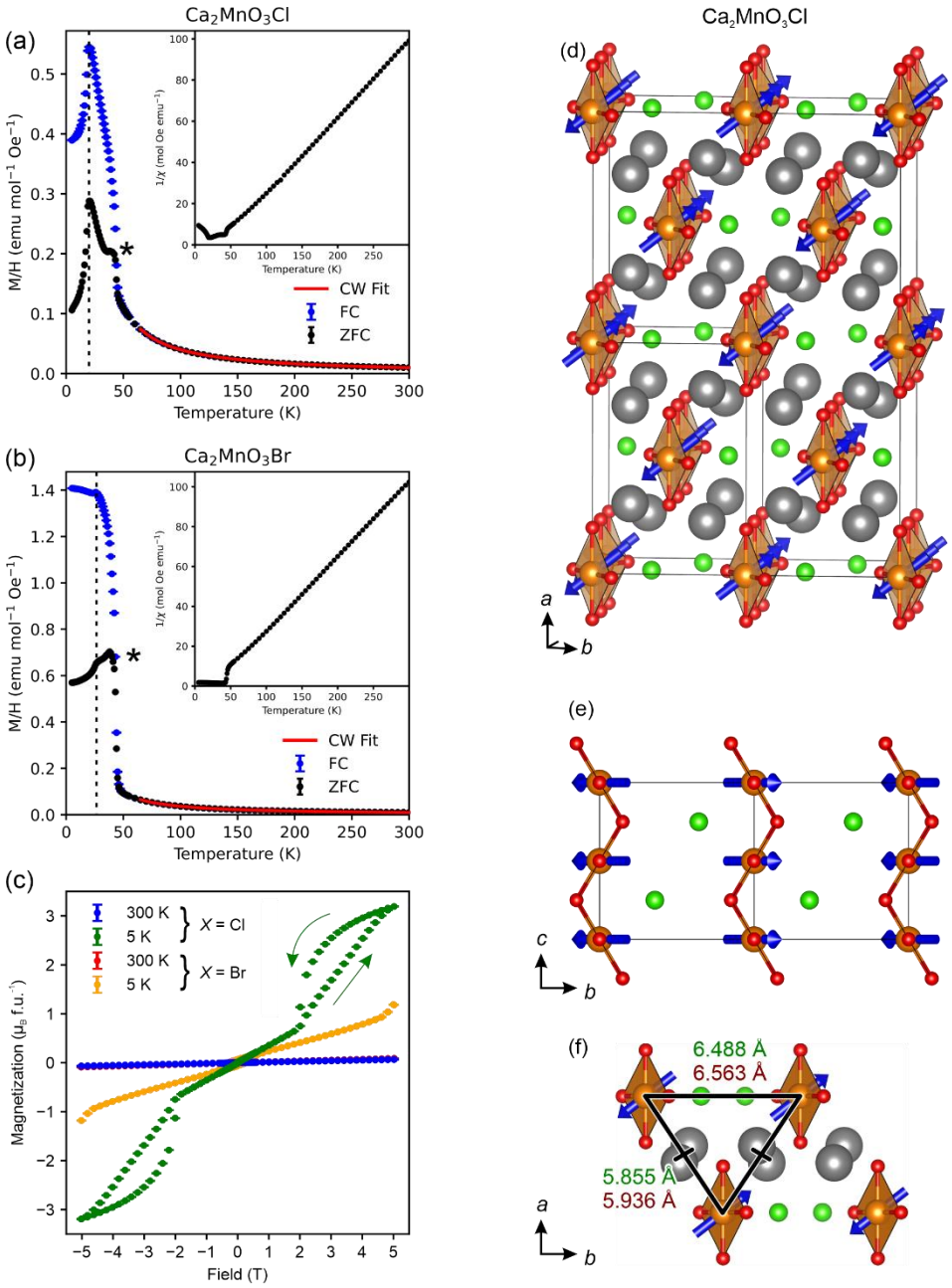

Figure 3. (a) Zero-field (ZFC) and field cooled (FC) magnetization data collected from Ca_2MnO_3Cl as a function of temperature under an applied field of 100 Oe. Inset: inverse susceptibility. (b) Zero-field (ZFC) and field cooled (FC) magnetization data collected from Ca_2MnO_3Br as a function of temperature under an applied field of 100 Oe. Inset: inverse susceptibility. (c) Magnetization data collected as a function of field from Ca_2MnO_3X (X = Cl, Br). In (a) and (b), the feature marked with an asterisk is assigned to a small amount of ferrimagnetic γ-Mn_2O_3 (< 1%) while the dashed line corresponds to the AFM ordering temperatures of Ca_2MnO_3X. (d) and (e) Refined magnetic structure of Ca_2MnO_3Cl. The smaller unit cell corresponds to the nuclear cell and the larger to the magnetic in the setting of the parent. (f) Separation between the chains at 100 K in Ca_2MnO_3Cl (green, upper values) and Ca_2MnO_3Br (brown, lower values).

Neutron powder diffraction data collected from both materials at 1.6 K contained additional reflections indicating long-range magnetic order. In both cases, these could be indexed using a propagation vector k = (½, ½, 0). There are only two possible maximal subgroups compatible with this propagation vector, one of which completely failed to account for the observed magnetic intensity. The magnetic structure shown in Figure 3 (d-f) and Figure S 7 (space group P_c2_1/c (14.82)) resulted in the best fit to the data.

The refined structure contains only a single magnetic site. Refined moments of 3.7(1) and 3.5(1) μ_B were obtained for X = Cl and Br respectively. Observed, calculated, and difference plots for the refinements against

data with λ = 2.53 Å are shown in Figure 2 (b) and S 6. Observed, calculated, and difference plots for the refinements against data with λ = 1.29 Å and the obtained refined parameters are given in the Supporting Information.

This structure preserves the *C* centering of the nuclear cell. During the refinement and despite the zigzag arrangement of MnO_4 square planes, the M_z component refined to 0 within error and was therefore fixed at this value, resulting in collinear moments on every site with a direction close to the [110] of the nuclear cell, perpendicular to the chain direction. The structure consists of an antiferromagnetic arrangement of ferromagnetic chains. Neighboring chains separated by halide ions are AFM, while those separated by calcium cations show both FM and AFM alignment.

Discussion

Structural Properties

Mixed systems containing oxide and heavy anions such as S, Se, Cl, Br, etc…) tend to adopt layered structures. This is due to the large differences in size and polarizability between the two anionic species (Hume-Rothery rules).[21] For example, substitution of chloride for oxide in materials adopting the n = 1 Ruddlesden-Popper (RP) structure type tends to result in oxychloride materials where the Cl^- anions replace the apical oxides in an ordered fashion as shown in the structures of $Sr_2M^{3+}O_3Cl$ (*M* = V, Mn, Fe, Co, and Ni) and $Ca_2Fe^{3+}O_3Cl$.[2–7] Further substitution results in the replacement of the remaining apical oxide as shown by the structures of $A_2Cu^{2+}O_2Cl_2$ (*A* = Ca, Sr) and $Sr_2Co^{2+}O_2Cl_2$.[8,9,22]

The Ca^{2+} cation is too small to be properly accommodated in the *A* sites of the RP structure without a structural distortion. This accounts for the relative paucity of Ca_2MO_3Cl phases, which were hereto known only for *M* = Fe.[7] This factor, combined with the strong Jahn-Teller effect characteristic of high spin Mn^{3+}, results in the observed crystal structure of Ca_2MnO_3X. This structure is related to that of the n = 1 RP phases, but with the halide anions replacing equatorial rather than apical oxide ions. A significant rotation of the Mn coordination environment is necessary to accommodate these, resulting in the zig-zag arrangement of MnO_4 square planes. The structure is further stabilized by the Jahn-Teller distortion typical of $3d^4$ Mn^{3+}.

Refined bond lengths, angles, and bond valence sum parameters from Ca_2MnO_3X are given in Table 2. The calcium cations occupy seven-coordinate sites (five oxide and two halide anions). The Mn cations are formally coordinated to oxide anions in a square planar environment with much longer interactions to halides in the apical sites. While the Mn-*X* bond lengths are significantly shorter than those found in other oxyhalides (c.f. 3.184 Å and 3.151 Å in Sr_2MnO_3Cl and $Sr_4Mn_3O_{8-x}Cl_2$ respectively), these bonds have a small contribution (~5%) to the final valence sum, indicating weak metal-halide interactions.[3]. The Mn-O bond lengths comparable to those found in other compounds containing square-planar Mn^{3+} (c.f. 1.924 Å in $YMn_3Al_4O_{12}$; 1.914 Å in $SrMn_7O_{12}$).[23,24]

Table 2. Selected refined bond lengths, angles, and bond valence sum (BVS) parameters from Ca_2MnO_3X at 100 K.

	X = Cl	*X* = Br
Ca-*X*	3.122(4) Å ×1 2.945(3) Å ×1	3.125(3) Å ×1 3.027(3) Å ×1
Ca-O1	2.250(4) Å ×1	2.253(4) Å ×1
Ca-O2	2.468(2) Å ×2 2.337(3) Å ×2	2.479(3) Å ×2 2.353(3) Å ×2
Ca BVS[25]	2.06	1.63
Mn-*X*	2.851(2) Å ×2	2.898(3) Å ×2
Mn-O1	1.909(3) Å ×2	1.915(2) Å ×2
Mn-O2	1.925(3) Å ×2	1.932(3) Å ×2
Mn BVS[25]	2.91	2.57
Mn-Mn intrachain	3.288(2) Å	3.285(2) Å
Mn-O1-Mn (α)	118.9(2) °	118.2(2) °

Magnetic Properties

At low temperatures, both Ca_2MnO_3X materials adopt long-range antiferromagnetic structures (T_N ~ 20 and 28 K for *X* = Cl and Br respectively). In both cases, the spins within each chain order ferromagnetically, and chains with intermediate *X* anions are antiferromagnetically arranged (Figure 3 (d-f) and Figure S 7). The lack of a correlation between the moment direction and orientation of the square planar coordination environment is indicative of weak single ion anisotropy.

The dominant interaction is expected to be the ferromagnetic intrachain interaction, as evidenced by the Weiss temperature. The long range 3d ordering is governed by the exchange between chains separated by the halide anions. Pairs of chains separated by Ca cations show both parallel and antiparallel arrangements (Figure 3 (f)) and therefore this interaction does not contribute to the total energy.

Interestingly, Ca_2MnO_3Br has a higher T_N (28 K vs 20 K for Ca_2MnO_3Cl) and metamagnetic transition field (4.8 T vs 2 T for Ca_2MnO_3Cl) despite a significantly greater separation between the spin chains (Figure 3 (f)). This behavior is similar to that observed in the manganese dihalides and their tetrahydrates (MnX_2 and $MnX_2{\cdot}4H_2O$) which have lower ordering temperatures for *X* = Cl than for *X* = Br (1.96 K vs 2.16 K and 1.62 K vs 2.12 K respectively).[26,27] The $MnX_2{\cdot}4H_2O$ phases also show spin flop transitions at low temperature, with much higher fields for *X* = Br than for *X* = Cl.[28] In $[(CH_3)_3NH]MnX_3{\cdot}4H_2O$ linear chain compounds, the strength of the exchange interaction is greater for *X* = Br than for *X* = Cl, resulting in high T_N for the Br compound (1.58 K vs. 0.98 K).[29,30]

It should be noted that there are very few examples of comparable $S = 2$ d^4 materials with similar 1-dimensional chains: the Cr^{2+} dihalides and Mn^{3+} trihalides and their respective solvent adducts tend to be unstable and/or air-sensitive.[30–33]

Conclusions

Two novel mixed anion compounds with formula Ca_2MnO_3X (X = Cl, Br) are reported and characterized. Both compounds contain 1-dimensional chains of corner-sharing Mn^{3+} square planes. At low temperatures, both materials adopt an overall long-range antiferromagnetic order in which the spins within each chain are ferromagnetically coupled. Both materials show spin flop transitions below T_N.

The X = Br phase shows a high T_N and H_C despite the increased separation between magnetic centers. This effect is ascribed to an enhancement of the anisotropic exchange interaction on substitution.

These materials highlight the role of ionic and electronic effects in stabilizing unusual structure types in mixed anion solid state compounds. The resulting materials contain rare examples of ferromagnetic $S = 2$ chains.

ASSOCIATED CONTENT

Supporting Information. Selected sections of the reciprocal space indexed in *Cmcm* space group of Ca_2MnO_3Cl, electrostatic potential map, tables of refined parameters, plots of the refinement against neutron powder diffraction data with $\lambda \sim 1.29$ Å. This material is available free of charge via the Internet at http://pubs.acs.org.

AUTHOR INFORMATION

Corresponding Author

* fabio.denis-romero@neel.cnrs.fr

Author Contributions

The manuscript was written through contributions of all authors. All authors have given approval to the final version of the manuscript.

ACKNOWLEDGMENT

The TEM facility JEOL NEOARM at CNRS Institut Néel was co-financed by the European Union under the European Regional Development Fund (ERDF, contract n° RA0023813).

REFERENCES

(1) Kageyama, H.; Hayashi, K.; Maeda, K.; Attfield, J. P.; Hiroi, Z.; Rondinelli, J. M.; Poeppelmeier, K. R. Expanding Frontiers in Materials Chemistry and Physics with Multiple Anions. *Nat Commun* **2018**, *9* (1), 772. https://doi.org/10.1038/s41467-018-02838-4.

(2) Sannes, J. A.; Kizhake Malayil, R. K.; Corredor, L. T.; Wolter, A. U. B.; Grafe, H.-J.; Valldor, M. Synthesis and Characterization of Oxide Chloride Sr_2VO_3Cl, a Layered S = 1 Compound. *ACS Omega* **2023**, *8* (15), 14233–14239. https://doi.org/10.1021/acsomega.3c01151.

(3) Knee, C. S.; Zhukov, A. A.; Weller, M. T. Crystal Structures and Magnetic Properties of the Manganese Oxide Chlorides Sr_2MnO_3Cl and $Sr_4Mn_3O_{8-y}Cl_2$. *Chem. Mater.* **2002**, *14* (10), 4249–4255. https://doi.org/10.1021/cm020280c.

(4) Hector, A. L.; Hutchings, J. A.; Needs, R. L.; Thomas, M. F.; Weller, M. T. Structural and Mössbauer Study of Sr_2FeO_3X (X = F, Cl, Br) and the Magnetic Structure of Sr_2FeO_3F. *J. Mater. Chem.* **2001**, *11* (2), 527–532. https://doi.org/10.1039/B008321F.

(5) McGlothlin, N.; Ho, D.; Cava, R. J. $Sr_3Co_2O_5Cl_2$ and Sr_2CoO_3Cl: Two Layered Cobalt Oxychlorides. *Materials Research Bulletin* **2000**, *35* (7), 1035–1043. https://doi.org/10.1016/S0025-5408(00)00299-3.

(6) Tsujimoto, Y.; Yamaura, K.; Uchikoshi, T. Extended Ni(III) Oxyhalide Perovskite Derivatives: Sr_2NiO_3X (X = F, Cl). *Inorg. Chem.* **2013**, *52* (17), 10211–10216. https://doi.org/10.1021/ic402008n.

(7) Kriworuschenko, B.; Kahlenberg, V. On the Symmetry of the n = 1 Ruddlesden-Popper Phase Ca_2FeO_3Cl. *Crystal Research and Technology* **2002**, *37* (9), 958–963. https://doi.org/10.1002/1521-4079(200209)37:9<958::AID-CRAT958>3.0.CO;2-F.

(8) Grande, B.; Müller-Buschbaum, Hk. Über Oxocuprate. XVII. Zur Kenntnis von $Ca_2CuO_2Cl_2$ und $Ca_2CuO_2Br_2$. *Z. Anorg. Allg. Chem.* **1977**, *429* (1), 88–90. https://doi.org/10.1002/zaac.19774290112.

(9) Knee, C. S.; Weller, M. T. Neutron Diffraction Study of Crystal Structure and Antiferromagnetic Order in Sr 2 Co O 2 X 2 (X = Cl , Br). *Phys. Rev. B* **2004**, *70* (14), 144406. https://doi.org/10.1103/PhysRevB.70.144406.

(10) Ackerman, J. F. The Preparation and Structures of the Alkaline Earth Iron Oxyhalides. *Journal of Solid State Chemistry* **1991**, *92* (2), 496–513. https://doi.org/10.1016/0022-4596(91)90356-M.

(11) Leib, W.; Müller-Buschbaum, Hk. Ein neuer Bautyp der Oxohalogenoferrate: $Ba_3Fe_2O_5Cl_2$ und $Ba_3Fe_2O_5Br_2$. *Z. Anorg. Allg. Chem.* **1985**, *521* (2), 51–56. https://doi.org/10.1002/zaac.19855210207.

(12) Schafer, H.; Wartenpfuhl, F.; Weise, E. Uber Titanchloride. V. Titan(III)-oxychlorid. *Z. Anorg. Allg. Chem.* **1958**, *295* (3–4), 268–280. https://doi.org/10.1002/zaac.19582950314.

(13) Haase, A.; Brauer, G. Vanadium Oxychloride. *Acta Cryst B* **1975**, *31* (10), 2521–2522. https://doi.org/10.1107/S0567740875007984.

(14) Christensen, A. N.; Johansson, T.; Quézel, S. Preparation and Magnetic Properties of CrOCl. *Acta Chem. Scand.* **1974**, *28a*, 1171–1174. https://doi.org/10.3891/acta.chem.scand.28a-1171.

(15) Lind, M. D. Refinement of the Crystal Structure of Iron Oxychloride. *Acta Cryst B* **1970**, *26* (8), 1058–1062. https://doi.org/10.1107/S0567740870003618.

(16) Buisson, G. Structure cristalline d'un oxychlorure de manganèse, $Mn_8O_{10}Cl_3$. *Acta Cryst B* **1977**, *33* (4), 1031–1034. https://doi.org/10.1107/S0567740877005317.

(17) Palatinus, L.; Brázda, P.; Jelínek, M.; Hrdá, J.; Steciuk, G.; Klementová, M. Specifics of the Data Processing of Precession Electron Diffraction Tomography Data and Their Implementation in the Program PETS2.0. *Acta Cryst B* **2019**, *75* (4), 512–522. https://doi.org/10.1107/S2052520619007534.

(18) Palatinus, L. The Charge-Flipping Algorithm in Crystallography. *Acta Cryst B* **2013**, *69* (1), 1–16. https://doi.org/10.1107/S2052519212051366.

(19) Palatinus, L.; Chapuis, G. SUPERFLIP – a Computer Program for the Solution of Crystal Structures by Charge Flipping in Arbitrary Dimensions. *J Appl Cryst* **2007**, *40* (4), 786–790. https://doi.org/10.1107/S0021889807029238.

(20) Petříček, V.; Palatinus, L.; Plášil, J.; Dušek, M. Jana2020 – a New Version of the Crystallographic Computing System Jana. *Zeitschrift für Kristallographie - Crystalline Materials* **2023**. https://doi.org/10.1515/zkri-2023-0005.

(21) Hume-Rothery, W.; Powell, H. M. On the Theory of Super-Lattice Structures in Alloys. *Zeitschrift für Kristallographie - Crystalline Materials* **1935**, *91* (1–6), 23–47. https://doi.org/10.1524/zkri.1935.91.1.23.

(22) Grande, B.; Müller-Buschbaum, Hk. Über Erdalkalimetalloxocuprate, VIII Zur Kenntnis von $Sr_2CuO_2Cl_2$. *Zeitschrift für anorganische und allgemeine Chemie* **1975**, *417* (1), 68–74. https://doi.org/10.1002/zaac.19754170110.

(23) Tohyama, T.; Saito, T.; Mizumaki, M.; Agui, A.; Shimakawa, Y. Antiferromagnetic Interaction between *A′*-Site Mn Spins in *A*-Site-Ordered Perovskite $YMn_3Al_4O_{12}$. *Inorganic Chemistry* **2010**, *49* (5), 2492–2495. https://doi.org/10.1021/ic9024876.

(24) Glazkova, Y. S.; Terada, N.; Matsushita, Y.; Katsuya, Y.; Tanaka, M.; Sobolev, A. V.; Presniakov, I. A.; Belik, A. A. High-Pressure Synthesis, Crystal Structures, and Properties of $CdMn_7O_{12}$ and $SrMn_7O_{12}$ Perovskites. *Inorg. Chem.* **2015**, *54* (18), 9081–9091. https://doi.org/10.1021/acs.inorgchem.5b01472.

(25) Brese, N. E.; O'Keeffe, M. Bond-Valence Parameters for Solids. *Acta Crystallographica Section B Structural Science* **1991**, *47* (2), 192–197. https://doi.org/10.1107/S0108768190011041.

(26) McGuire, M. Crystal and Magnetic Structures in Layered, Transition Metal Dihalides and Trihalides. *Crystals* **2017**, *7* (5), 121. https://doi.org/10.3390/cryst7050121.

(27) Westphal, C. H.; Becerra, C. C. Antiferromagnetism in $Mn(Br_{1-x}Cl_x)_2.4H_2O$: A System with Controllable Anisotropy. *J. Phys. C: Solid State Phys.* **1980**, *13* (21), L527–L529. https://doi.org/10.1088/0022-3719/13/21/006.

(28) C H Westphal; C C Becerra. The Magnetic Phase Diagrams of $Mn(Br_{1-x}Cl_x)_2.4H_2O$ Antiferromagnets. *J. Phys. C: Solid State Phys.* **1982**, *15* (30), 6221–6232. https://doi.org/10.1088/0022-3719/15/30/016.

(29) *Extended Interactions between Metal Ions: In Transition Metal Complexes*; Interrante, L. V., Ed.; ACS Symposium Series; AMERICAN CHEMICAL SOCIETY: WASHINGTON, D. C., 1974; Vol. 5. https://doi.org/10.1021/bk-1974-0005.

(30) Carlin, R. L. *Magnetochemistry*; Springer Berlin Heidelberg: Berlin, Heidelberg, 1986. https://doi.org/10.1007/978-3-642-70733-9.

(31) Muetterties, L. *Inorganic Syntheses, Volume 10*; Wiley, 1967.

(32) Greenwood, N. N.; Earnshaw, A. *Chemistry of the Elements*; Elsevier, 1997; p 1341. https://doi.org/10.1016/C2009-0-30414-6.

(33) Nachtigall, O.; Pataki, A.; Molski, M.; Lentz, D.; Spandl, J. Solvates of Manganese Trichloride Revisited – Synthesis, Isolation, and Crystal Structure of $MnCl_3(THF)_3$. *Zeitschrift für anorganische und allgemeine Chemie* **2015**, *641* (6), 1164–1168. https://doi.org/10.1002/zaac.201500106.

Insert Table of Contents artwork here